


SCIENTIFIC REPORTS



OPEN

Enhanced photoelectrochemical properties of nanocrystalline TiO₂ electrode by surface sensitization with Cu_xO quantum dots

Jiajia Tao¹, Zhaoqi Sun¹, Yunlang Cheng¹, Miao Zhang¹, Jianguo Lv², Shiwei Shi¹, Gang He¹, Xishun Jiang³, Xiaoshuang Chen⁴, Xingzhi Wang¹, Zhuang Wang¹ & Zezhou Gong¹

Nanoporous anatase TiO₂ films were fabricated by a screen-printing method, and Cu_xO quantum dots (QDs) were deposited on the TiO₂ films through successive ionic layer adsorption and reaction (SILAR). The amount of Cu_xO QDs on the TiO₂ films are controlled by changing the number of SILAR cycles. The morphology, microstructure, optical, and photoelectrochemical properties of different Cu_xO sensitized TiO₂ films (Cu_xO/TiO₂) were investigated in detail. The nanoporous TiO₂ film offers a large surface area for anchoring QDs. QD deposited samples exhibited a significant improvement in photoelectrochemical performance than the bare of TiO₂. Cu_xO/TiO₂, prepared with 7 SILAR cycles, showed the best photoelectrochemical properties, where the photocurrent density was enhanced to 500.01 μA/cm² compared with 168.88 μA/cm² of bare TiO₂ under visible light. These results indicate that the designed Cu_xO/TiO₂ structure possesses superior charge separation efficiency and photoelectrochemical properties.

Titanium dioxide (TiO₂) has attracted great interest for water splitting^{1,2}, quantum dot-sensitized solar cells^{3,4}, optical sensors^{5,6}, photocatalytic degradation⁷ and other applications^{8–10}, due to its unique optical and photoelectric properties. Nevertheless, the intrinsic band gap of TiO₂ (3.0 eV for rutile and 3.2 eV for anatase) limits its photoelectrochemical utility¹¹. Specifically, the wide band gap restricts the photoresponse of TiO₂ to only ultraviolet region, with the wavelengths below 380 nm, which constitutes less than 5% of the solar spectrum. Therefore, many studies have been conducted to extend the TiO₂ optical absorption range to the visible light region, in order to expand the portion of the solar spectrum for which TiO₂ can be utilized.

In recent years, quantum dots (QDs) have become increasingly attractive for similar applications as TiO₂, because of their unique electronic and optical properties^{12,13}, such as their high extinction coefficients^{14,15}, tunable band gap^{16,17}, multiple exciton generation^{18,19}, and an expandable optical absorption range by controlling particle size^{20,21}. Various QDs, including CdS²², CdSe²³, PbS²⁴, PbSe²⁵, and so on^{26,27}, have been thoroughly studied. Although these studies have demonstrated that QDs-sensitized TiO₂ can efficiently absorb visible light, inherent disadvantages of these QDs, such as a fixed visible light absorption range, the toxicity of elements, and the use of rare elements, limit their applications in biology, environment, medicine, and solar cells²⁸. As a result, it is important to discover environmentally friendly QD materials. Recently, the development of copper oxides as both the core photocatalytic material and the photoelectrochemical material has drawn increasing amounts of attention^{29–31}. Copper materials, which are multifunctional p-type semiconductors, with a band gap ranging between 1.5 and 2.4 eV³², are environmentally friendly and can absorb in the visible light region^{33,34}. Until now, to the best of our knowledge, previous studies have not reported the surface sensitization of a nanocrystalline TiO₂ electrode with Cu_xO QDs.

Unlike many syntheses of QDs, such as electrode deposition³⁵, photocatalytic reduction³⁶, and sol-gel method³⁷, our study uses a novel technique to fabricate Cu_xO QDs via successive ionic layer adsorption and

¹School of Physics & Materials Science, Anhui University, Hefei, 230601, P.R. China. ²School of Electronic & Information Engineering, Hefei Normal University, Hefei, 230601, P.R. China. ³School of Mechanical & Electronic Engineering, Chuzhou University, Chuzhou, 239000, P.R. China. ⁴National Laboratory for Infrared Physics, Shanghai Institute of Technical Physics, Chinese Academy of Sciences, Shanghai, 200083, P.R. China. Correspondence and requests for materials should be addressed to Z.S. (email: szq@ahu.edu.cn)

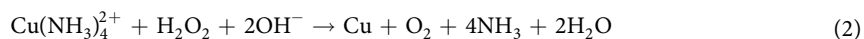
reaction (SILAR) method³⁸. SILAR is a simple fabrication methodology that combines successive layer adsorption with chemical redox reaction. The typical process involves successively immersing the TiO₂ materials in Cu(NH₃)₄²⁺ and H₂O₂ aqueous solutions successively for as many cycles as desired to achieve a uniform deposition of Cu_xO QDs. Not only is the overall process environmentally friendly, cost-effective, and can be carried out in normal atmospheric pressure and room temperature, but the density of QDs can also be easily controlled by merely varying the number of deposition cycles.

In this study, we report the preparation of nanoporous anatase TiO₂ films on transparent conductive fluorine-doped tin oxide (FTO) substrates by screen-printing and the subsequent deposition of Cu_xO QDs on the TiO₂ films via SILAR. The number of deposition cycles, and thus QD loading density, was varied to investigate the effect on the photoelectrochemical properties of nanocrystalline TiO₂ electrode and derive the optimal density of Cu_xO QDs that enhanced the photoelectrochemical activity. The sample was also recycled 7 times to demonstrate its improved absorbance in the visible range and enhanced photoelectrochemical properties.

Experimental

Preparation of TiO₂ films. All the chemical reagents were used as received. The colloidal were prepared by hydrolysis of titanium tetraisopropoxide as described by elsewhere³⁹. The TiO₂ films were synthesized directly on transparent fluorine-doped tin oxide (FTO, TEC-8, LOF) conducting glass substrates by screen-printing, followed by calcining the samples at 500 °C for 30 min in air.

Immobilization of Cu_xO quantum dots onto TiO₂ films. The Cu_xO QDs were deposited onto the TiO₂ photoanodes *in situ* by successive SILAR cycles. For Cu_xO deposition, the TiO₂ photoanodes were successively immersed in two different solutions for 5 min in each solution, first, in Cu(NH₃)₄²⁺ and second in H₂O₂ aqueous solutions. Following each immersion, the TiO₂ photoanodes were rinsed with deionized water. The Cu(NH₃)₄²⁺ were resulting from Cu(AC)₂ and NH₃•H₂O. These sequential steps are considered as one SILAR cycle. The SILAR cycle was repeated for 0, 3, 5, 7, and 9 times. Samples are denoted as S0, S3, S5, S7, and S9, respectively. The relevant reactions for preparing Cu_xO QDs can be written as follows⁴⁰:



Characterization techniques. Microstructures and the crystallinity of Cu_xO sensitized TiO₂ films were characterized by field-emission scanning electron microscopy (FE-SEM, Hitachi, S4800), transmission electron microscopy (TEM), high resolution transmission electron microscopy (HR-TEM) (TEM, JME-2100, Japan), and X-ray diffraction (XRD, MAC, M18XHF) using CuKα radiation (1.54 Å). Absorption spectra were obtained by a UV-Vis spectrophotometer (UV-2550, Shimadzu). Photoluminescence (PL) and Raman spectra were recorded by a micro-Raman spectroscopy system (Renishaw PLC in Via-Reflex). X-ray photoelectron spectroscopy (XPS, Thermo, ESCALAB 250) was employed to analyze the surface composition of the samples. The elemental distributions and concentrations were analyzed by Energynergy dispersive spectroscopy (EDS, Oxford Inca) accompanying the FE-SEM.

Photoelectrochemical measurements. Photoelectrochemical measurements were carried out in a three-electrode configuration with the as-prepared sample as the working electrode, Pt foil as the counter electrode, and saturated Ag/AgCl as the reference electrode⁴¹. A 0.1 M Na₂SO₃ aqueous solution was used as the electrolyte. Photocurrent measurements were taken as a function of voltage by an electrochemistry workstation (CHI 660D, Shanghai Chenhua instrument). The working electrode was illuminated by a 300 W Xe lamp. An ultraviolet cutoff filter was inserted in between the light source and the quartz cell to exclude UV light with wavelength below 420 nm. Photoresponses of the different samples were determined by using a light on-off cycle of 60 s at a bias of 0 V versus the Ag/AgCl electrode.

Results and Discussion

XRD patterns. Figure 1 shows XRD patterns of S0 and S9. The XRD pattern of the substrate (FTO) was used as a reference. After the TiO₂ products were formed on the FTO substrates, all FTO diffraction peaks became weaker. Both S0 and S9 samples have similar patterns, in that they display three peaks at 2θ = 36.02°, 62.56°, and 69.01°. These peaks can be attributed to the (101), (002), and (301) diffraction peaks of anatase TiO₂, respectively, as they are in good agreement with the standard pattern of anatase TiO₂ (PDF#65-1119). In addition, the diffraction peaks of Cu_xO QDs are not observed in S9, implying the low content and small size of QDs. Therefore, we can conclude that the formation of Cu_xO QDs does not influence the crystalline structure of the TiO₂ electrodes.

Morphological analysis. Figure 2 presents SEM images of TiO₂ films coated with Cu_xO QDs. The magnification and high magnification SEM images (Fig. 2a and b) show that the TiO₂ film is porous and uniform. Figure 2c–f shows SEM images of the TiO₂ after depositing 3, 5, 7, and 9 cycles of Cu_xO QDs. No morphological changes were observed among the samples deposited with Cu_xO QDs, due to the low content and small size of the Cu_xO QDs; however, EDS data of S7 (Fig. 2(g)) reveal that the sample consists of Ti, O, and Cu elements, confirming the presence of Cu_xO QDs.

TEM and SAED characterization was employed to examine the crystal structure and growth direction of TiO₂ as well as the particle size of the Cu_xO QDs. Figure 3(a) shows that Cu_xO QDs were in contact with the TiO₂ film. The size of TiO₂ nanoparticles and Cu_xO QDs were approximately 34 nm and 10 nm, respectively. When the

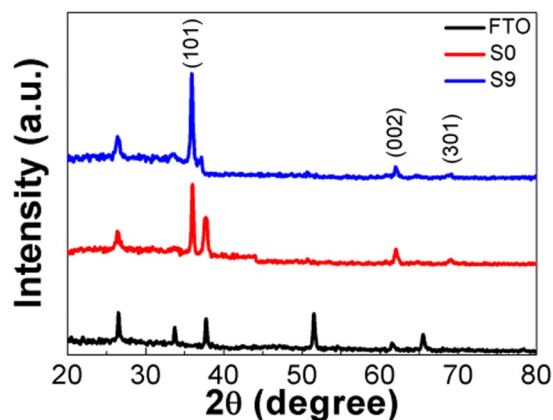


Figure 1. XRD patterns of S0, S9, and FTO substrate.

imaging was focused around the TiO_2 and $\text{TiO}_2/\text{Cu}_x\text{O}$ interface, various crystalline facets were clearly observed, as shown in Fig. 3b and c. The larger crystalline region in Fig. 3b was confirmed to be TiO_2 . The observed lattice plane spacings are 0.17 nm and 0.34 nm corresponding to the (211) and (110) planes of anatase TiO_2 . Above the anatase TiO_2 crystallites, we also observed the interplanar spacings of 0.21 and 0.23 nm (Fig. 3c), which could be indexed to elementary Cu (111) ($d = 0.21$ nm), CuO (111) ($d = 0.23$ nm), or Cu_2O (002) ($d = 0.21$ nm). In addition, the SAED pattern in Fig. 3d demonstrates that the TiO_2 electrodes exhibit a single crystal structure.

XPS analysis. In order to clarify the elemental composition and valence state of Cu_xO QDs, XPS characterizations were conducted. As shown in Fig. 4a, the general survey spectrum for Cu_xO QDs modified TiO_2 electrodes contains Cu, O, Ti, and C elements. The small amount of carbon could have resulted from adventitious hydrocarbons from the XPS instrument itself and can be taken as the standard signal for the correction of other peaks⁴². From the Ti 2p spectrum (Fig. 4b), two main peaks at bonding energies of 458.6 and 461.4 eV were assigned to Ti 2p_{3/2} and Ti 2p_{1/2}, respectively^{43,44}. Figure 4c shows a representative Cu 2p core level XPS spectrum with two peaks at 933.2 and 953.0 eV for atmospheric conditions at room temperature, and the oxidation products include Cu_2O and CuO^{45,46}. Furthermore, two fitted peaks (Fig. 4d) from the O 1s spectrum are observed around 529.7 and 531.9 eV, which can be assigned to the lattice oxygen and surface hydroxyl oxygen of TiO_2 ⁴⁷, respectively.

UV-Visible absorption spectra. Figure 5 shows the absorption spectra of TiO_2 electrodes sensitized with different SILAR cycles of Cu_xO QDs. The average absorbance can be calculated and the results are listed in Table 1. It can be seen that with an increase in the number of SILAR cycles, the absorbance increases at wavelengths 400 to 700 nm. This can be attributed to the SPR of Cu QDs and narrow band gap of CuO and Cu_2O ⁴⁸. In addition, the red-shift of the absorption edge of $\text{Cu}_x\text{O}/\text{TiO}_2$ is due to the broadening of size distribution of Cu_xO QDs⁴⁹. Based on the UV-Visible absorption spectra, a plot of $(\alpha h\nu)^2$ versus energy ($h\nu$) is shown in Fig. 6, and the Eg values of different Cu_xO samples are shown in Table 1. It can be seen that the absorption bands of $\text{Cu}_x\text{O}/\text{TiO}_2$ show large variation, which change from 2.90 to 2.50 eV. The band gap of $\text{Cu}_x\text{O}/\text{TiO}_2$ (S9) was 2.50 eV, which was smaller than that of TiO_2 (2.90 eV). These results suggest that the formation of the $\text{Cu}_x\text{O}/\text{TiO}_2$ nanostructures decreased the recombination of photogenerated electrons and holes and improved the photoelectrochemical ability of the TiO_2 electrodes.

PL spectra. To investigate charge transfer between photogenerated electrons and hole pairs, photoluminescence (PL) emission spectroscopy was used to measure the recombination of free charge carriers. The emission peaks at 420 and 475 nm are assigned to exciton-caused PL resulting from band edge free excitons and defects of TiO_2 ⁵⁰. PL peak intensity correlates directly with the defect densities in materials. The higher PL intensity typically indicates a higher recombination rate of the photo-generated electrons and holes⁵¹. As shown in Fig. 7, the PL intensity of $\text{Cu}_x\text{O}/\text{TiO}_2$ reveals a significant decrease with increasing Cu_xO QDs. This is due to a decrease of radiative recombination processes⁵². When the Cu_xO QDs are deposited on TiO_2 electrodes, TiO_2 can easily bond with the Cu_xO QDs to form the $\text{Cu}_x\text{O}/\text{TiO}_2$ composites. The photo-induced electrons can be trapped in the Cu 2p energy level below the conduction band in the $\text{Cu}_x\text{O}/\text{TiO}_2$ composites, which inhibit the recombination of electron-hole pairs. The intensity of the peaks at 420 and 475 nm are the lowest for S7, which exhibit high quantum efficiency and higher photoelectrochemical properties.

Photoelectrochemical studies. Figure 8 shows the time-dependent photocurrent curves of $\text{Cu}_x\text{O}/\text{TiO}_2$ under visible light illumination. It is generally known that transient photocurrent always reflect the transfer and separation of photoinduced charge carriers under intermittent illumination. As the light is turned on, the photocurrent values increase while the photocurrent values decrease rapidly as the light is turned off. This suggests that all samples have good reproducibility. In addition, photocurrents increase with more SILAR cycles, which indicate that the photocurrent of $\text{Cu}_x\text{O}/\text{TiO}_2$ have a significant enhancement compared to bare TiO_2 . Moreover, after 7 SILAR cycles, the sample shows the highest photocurrent value of ca. $138 \mu\text{A}/\text{cm}^2$, which is about 13 times higher than that for bare TiO_2 . Nevertheless, when the SILAR cycles increase to 9, the photocurrent value

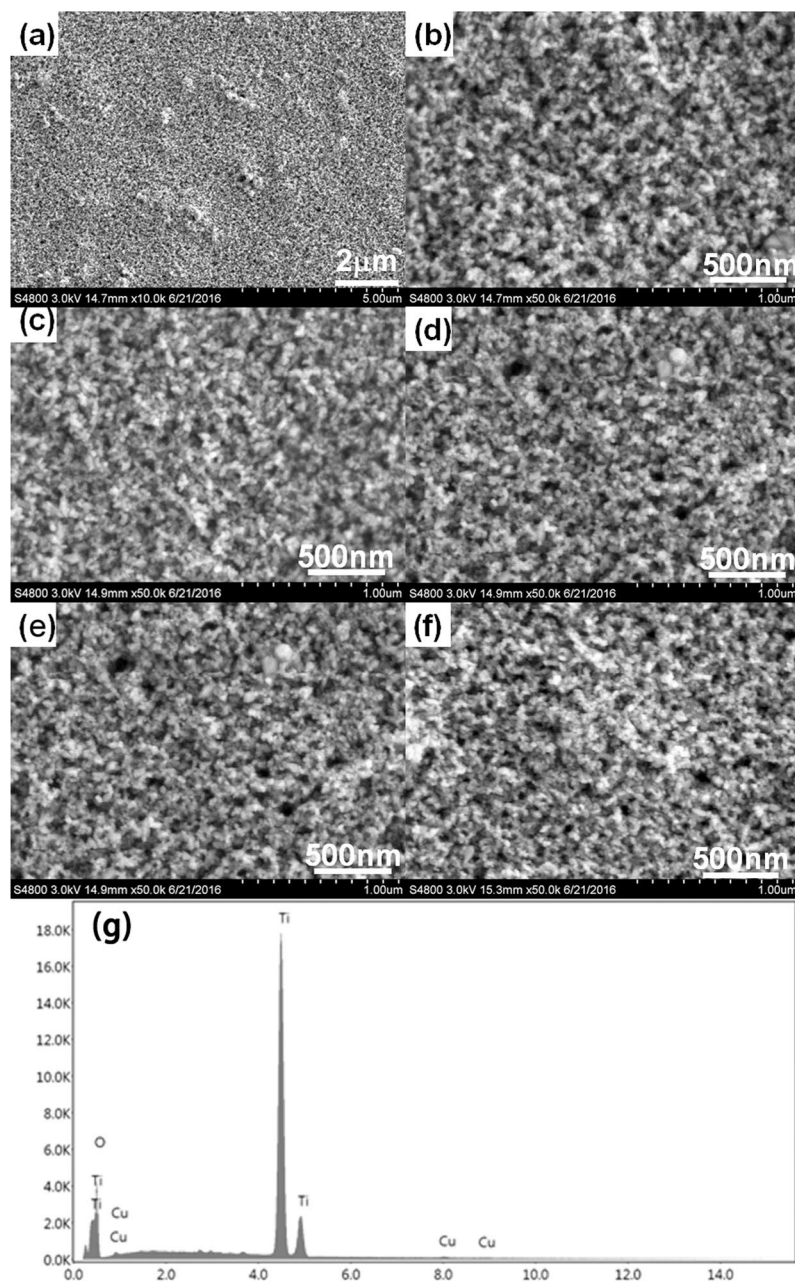


Figure 2. SEM images of S0 (a) close-up view (b) high resolution view (c) S3, (d) S5, (e) S7, (f) S9; and (g) EDS spectrum of S7.

decreases to ca. $120 \mu\text{A}/\text{cm}^2$. The increase in photocurrent may be attributed to the stronger SPR effect of Cu_xO QDs, which improves the light absorption of TiO_2 . With more than 9 SILAR cycles, the aggregation of Cu_xO QDs lead to a large particle size of Cu_xO QDs, which could block the surface active sites of TiO_2 and act as potential barrier of charge transfer, resulting in a decrease of the photoelectrochemical properties^{53–56}.

Figure 9 shows the LSV curves of the different samples in the dark and under light irradiation. Photocurrent values are shown in Table 1. The photocurrents of the $\text{Cu}_x\text{O}/\text{TiO}_2$ samples improved compared with that of bare TiO_2 , suggesting that the $\text{Cu}_x\text{O}/\text{TiO}_2$ exhibit a stronger ability to separate photo-generated electron-hole pairs. The $\text{Cu}_x\text{O}/\text{TiO}_2$ prepared with a different number of SILAR cycles (0, 3, 5, 7 and 9 times) exhibited photocurrent values of 168.88, 248.95, 390.98, 500.01, and $424.15 \mu\text{A}/\text{cm}^2$ at 1.0 V (vs Ag/AgCl) under visible light irradiation, respectively. Clearly, photocurrent densities of the $\text{Cu}_x\text{O}/\text{TiO}_2$ first increase then decrease with increasing the SILAR cycles. The S7 showed the strongest photocurrent value, and exhibits the best photoelectrochemical property, which is consistent with the PL results. When 9 SILAR cycles were used, the Cu_xO QDs aggregated to form a compact granular morphology, resulting in a lower surface area and reduced photocurrent⁵⁷.

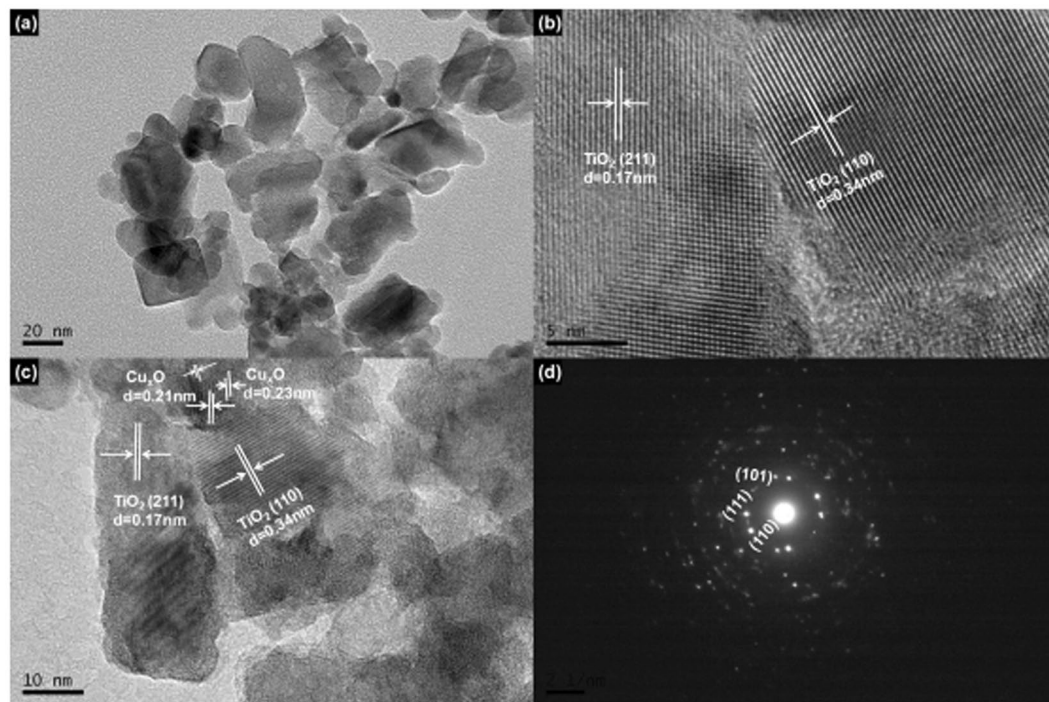


Figure 3. (a) TEM images of $\text{Cu}_x\text{O}/\text{TiO}_2$ (S7), (b) HRTEM of TiO_2 (S0), (c) HRTEM of $\text{Cu}_x\text{O}/\text{TiO}_2$ (S7), and SAED pattern of the same $\text{Cu}_x\text{O}/\text{TiO}_2$ in part (a).

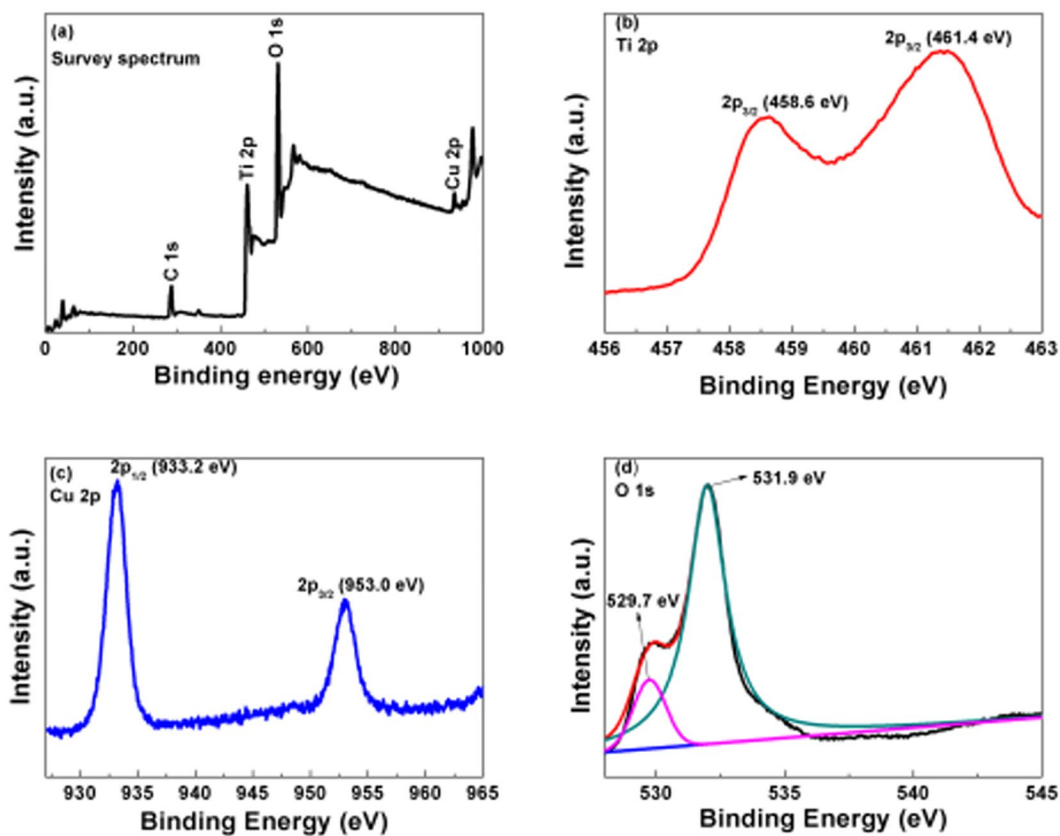


Figure 4. XPS spectra of S7: (a) Survey spectrum (b) Ti 2p, (c) Cu 2p, and (d) O 1s.

Samples	Average absorbance (a.u.)	Band gap (eV)	Photocurrent values (dark) ($\mu\text{A}/\text{cm}^2$)	Photocurrent values (light) ($\mu\text{A}/\text{cm}^2$)
S0	0.68	2.98	37.60	168.88
S3	0.82	2.75	97.47	248.95
S5	0.89	2.69	123.79	390.98
S7	0.92	2.63	166.74	500.01
S9	0.94	2.50	145.30	424.15

Table 1. The average absorbance with 400–700 nm, band gap, and photocurrent values of $\text{TiO}_2/\text{Cu}_x\text{O}$ electrodes.

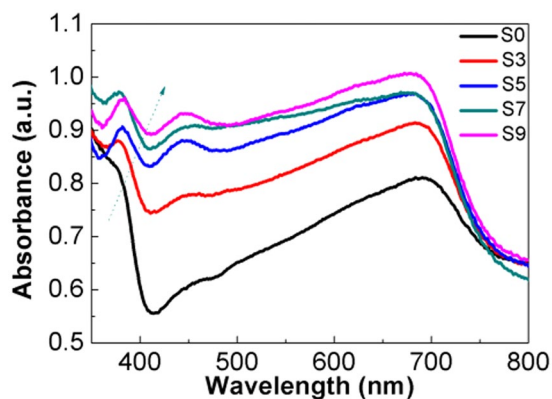


Figure 5. UV-Visible absorption spectra of $\text{Cu}_x\text{O}/\text{TiO}_2$ prepared with different SILAR cycles.

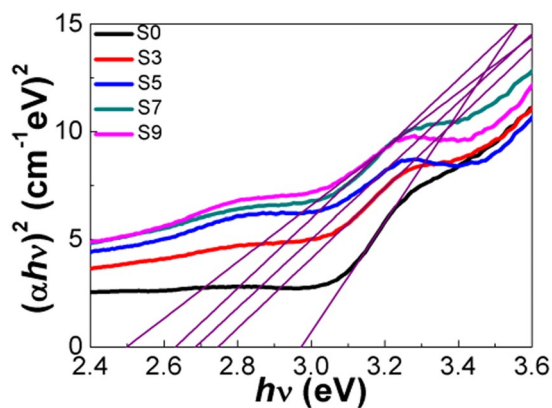


Figure 6. Plots of $(\alpha h\nu)^2$ versus energy ($h\nu$) for $\text{Cu}_x\text{O}/\text{TiO}_2$ prepared with different SILAR cycles.

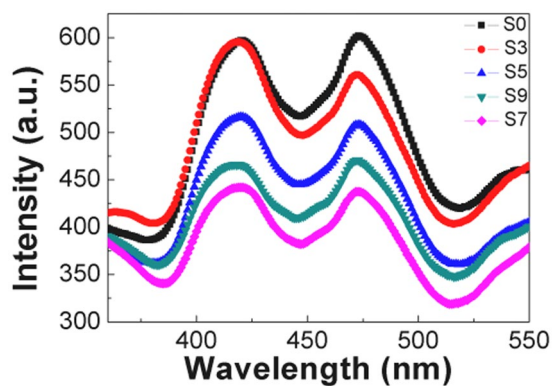


Figure 7. PL spectra of different samples.

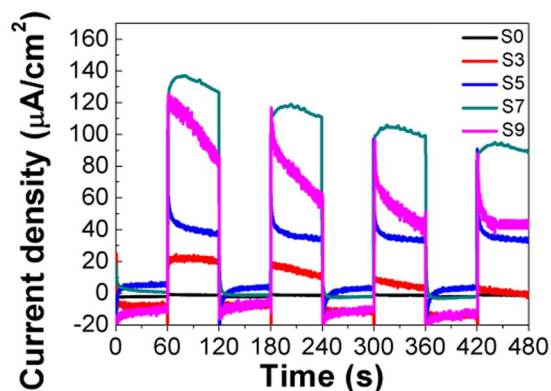


Figure 8. Transient photocurrents of $\text{Cu}_x\text{O}/\text{TiO}_2$ prepared with different SILAR cycles.

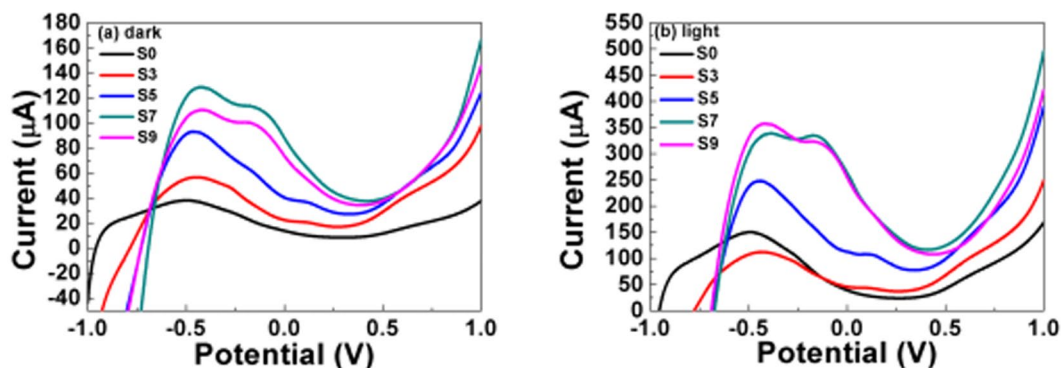


Figure 9. LSV spectra of $\text{Cu}_x\text{O}/\text{TiO}_2$ electrodes in dark and under visible light irradiation.

Conclusions

In summary, Cu_xO QDs are deposited on the nanoporous anatase TiO_2 films by a screen-printing method, followed by successive ionic adsorption and reaction (SILAR). The microstructure, morphology, and loading amounts of the Cu_xO QDs on the TiO_2 films are controlled by changing the number of SILAR cycles. The $\text{Cu}_x\text{O}/\text{TiO}_2$ absorbs more light and exhibits enhanced photoelectrochemical properties compared to bare TiO_2 . Moreover, under visible light illumination, the TiO_2 sensitized with 7 SILAR cycles of Cu_xO QDs shows the best photoelectrochemical properties, where the photocurrent density is increased to $500.01 \mu\text{A}/\text{cm}^2$, 2.96 times higher than the bare TiO_2 electrode with $168.88 \mu\text{A}/\text{cm}^2$. The superior photoelectrochemical properties of the $\text{Cu}_x\text{O}/\text{TiO}_2$ nanostructures could be ascribed to the large surface area of nanoporous TiO_2 electrode and the SPR effect of Cu_xO QDs. The electrode design of $\text{Cu}_x\text{O}/\text{TiO}_2$ will be beneficial for application of solar energy conversion and wastewater degradation.

References

- Fujishima, A. & Honda, K. Electrochemical photolysis of water at a semiconductor electrode. *Nature* **238**, 37–38 (1972).
- Dinh, C. T., Nguyen, T. D., Kleitz, F. & Do, T. O. Shape-controlled synthesis of highly crystalline titania nanocrystals. *ACS Nano* **3**, 3737–3743 (2009).
- Wang, S. M. *et al.* CdS and CdSe quantum dot co-sensitized nanocrystalline TiO_2 electrode: Quantum dot distribution, thickness optimization, and the enhanced photovoltaic performance. *J. Power Sources* **273**, 645–653 (2015).
- Hochbaum, A. I. & Yang, P. Semiconductor nanowires for energy conversion. *Chem. Rev.* **110**, 527–546 (2010).
- Zhang, Q., Yodyingyong, S., Xi, J., Myers, D. & Cao, G. Oxide nanowires for solar cell applications. *Nanoscale* **4**, 1436–1445 (2012).
- He, X. L., Cai, Y. Y., Zhang, H. M. & Liang, C. H. Photocatalytic degradation of organic pollutants with Ag decorated free-standing TiO_2 nanotube arrays and interface electrochemical response. *J. Mater. Chem.* **21**, 475–480 (2011).
- Song, Y. Y., Stein, F. S., Berger, S. & Schmuki, P. TiO_2 nano test tubes as a self-cleaning platform for high-sensitivity immunoassays. *Small* **6**, 1180–1184 (2010).
- Salari, M. *et al.* Enhancement of the electrochemical capacitance of TiO_2 nanotube arrays through controlled phase transformation of anatase to rutile. *Phys. Chem. Chem. Phys.* **14**, 4770–4779 (2012).
- Agosta, R. *et al.* Electrochemical assessment of the band-edge positioning in shape-tailored TiO_2 -nanorod-based photoelectrodes for dye solar cells. *J. Phys. Chem. C* **117**, 2574–2583 (2013).
- Gao, Z. D. *et al.* Nickel hydroxide nanoparticle activated semi-metallic TiO_2 nanotube arrays for nonenzymatic glucose sensing. *Chem. A Eur. J* **19**, 15530–15534 (2013).
- Labiadh, H. *et al.* Preparation of Cu-doped ZnS QDs/ TiO_2 nanocomposites with high photocatalytic activity. *Appl. Catal. Environ. B* **144**, 29–35 (2014).
- Sambur, J. B., Riha, S. C., Choi, D. & Parkinson, B. A. Influence of surface chemistry on the binding and electronic coupling of CdSe quantum dots to single crystal TiO_2 surfaces. *Langmuir* **26**, 4839–4347 (2010).

13. Jung, M. H. & Kang, M. G. Enhanced photo-conversion efficiency of CdSe-ZnS core-shell quantum dots with Au nanoparticles on TiO₂ electrodes. *J. Mater. Chem.* **21**, 2694–2700 (2011).
14. Semonin, O. E. *et al.* Peak external photocurrent quantum efficiency exceeding 100% via MEG in a quantum dot solar cell. *Science* **334**, 1530–1533 (2011).
15. Gao, M. *et al.* Strongly photoluminescent CdTe nanocrystals by proper surface modification. *J. Phys. Chem. B.* **102**, 8360–8363 (1998).
16. Yang, H., Holloway, P. H. & Ratna, B. B. Photoluminescent and electroluminescent properties of Mn-doped ZnS nanocrystals. *J. Appl. Phys.* **93**, 586–592 (2003).
17. Zalfani, M., Mahdouani, M., Bourguiga, R. & Su, B. L. Experimental and theoretical study of optical properties and quantum size phenomena in the BiVO₄/TiO₂ nanostructures. *Superlattices Microstruct.* **83**, 730–744 (2015).
18. Santra, P. K. & Kamat, P. V. Mn-doped quantum dot sensitized solar cells: a strategy to boost efficiency over 5%. *J. Am. Chem. Soc.* **134**, 2508–2511 (2012).
19. Sharma, S. N., Kohil, S. & Rastogi, A. C. Quantum confinement effects of CdTe nanocrystals sequestered in TiO₂ matrix: Effect of oxygen incorporation. *Phys. E* **25**, 554–561 (2005).
20. Khan, S. U. M., Al-Shahry, M. & Ingler, W. B. Efficient photochemical water splitting by a chemically modified n-TiO₂. *Science* **297**, 2243–2245 (2002).
21. Asahi, R., Morikawa, T., Ohwaki, T., Aoki, K. & Taga, Y. Visible-light photocatalysis in nitrogen-doped titanium oxides. *Science* **293**, 269–271 (2001).
22. Wang, H. *et al.* CdS quantum dots-sensitized TiO₂ nanorod array on transparent conductive glass photoelectrodes. *J. Phys. Chem. C* **114**, 16451–16455 (2010).
23. Luo, J. *et al.* Homogeneous photosensitization of complex TiO₂ nanostructures for efficient solar energy conversion. *Sci. Rep.* **2**, 451 (2012).
24. Etgar, L. *et al.* Light energy conversion by mesoscopic PbS quantum dots-TiO₂ heterojunction solar cells. *ACS Nano* **6**, 3092–3099 (2012).
25. Tisdale, W. A. *et al.* Hot-electron transfer from semiconductor nanocrystals. *Science* **328**, 1543–1547 (2010).
26. Zaban, A., Mičić, Q. I., Gregg, B. A. & Nozik, A. J. Photosensitization of nanoporous TiO₂ electrodes with InP quantum dots. *Langmuir* **14**, 3153–3156, (1998).
27. Yu, P. *et al.* Nanocrystalline TiO₂ solar cells sensitized with InAs quantum dots. *J. Phys. Chem. B* **110**, 25451–25454 (2006).
28. Wang, Q. Y., Qiao, J. L., Zhou, J. & Gao, S. M. Fabrication of CuInSe₂ quantum dot sensitized TiO₂ nanotube arrays for enhancing visible light photoelectrochemical performance. *Electrochim. Acta* **167**, 470–475 (2015).
29. Barreca, D. *et al.* Tailored vapor-phase growth of CuO_x-TiO₂ (x=2) nanomaterials decorated with Au particles. *Langmuir* **27**, 6409–6417 (2011).
30. Barreca, D. *et al.* Novel synthesis and gas sensing performances of CuO-TiO₂ functionalized with Au nanoparticles. *J. Phys. Chem. C* **115**, 10510–10517 (2011).
31. Heciak, A., Morawski, A. W., Grzmil, B. & Mozia, S. Cu-modified TiO₂ photocatalysts for decomposition of acetic acid with simultaneous formation of C1-C3 hydrocarbons and hydrogen. *Appl. Catal. B Environ* **140–141**, 108–114 (2013).
32. Nagaoka, K., Ueyama, J. & Ogura, K. Photoelectrochemical behavior of electrodeposited CuO and Cu₂O thin films on conducting substrates. *J. Electrochem. Soc.* **151**, C661–C665 (2004).
33. Sun, Q., Li, Y., Sun, X. & Dong, L. An improved photoelectrical performance of single-crystal TiO₂ nanorod arrays by surface sensitization with copper quantum dots. *ACS Sustain. Chem. Eng.* **1**, 798–804 (2013).
34. Hua, Z. L. *et al.* Copper nanoparticles sensitized TiO₂ nanotube arrays electrode with enhanced photoelectrocatalytic activity for diclofenac degradation. *Chem. Eng. J.* **283**, 514–523 (2016).
35. Tsui, L. K. & Zangari, G. Modification of TiO₂ nanotubes by Cu₂O for photoelectrochemical, photocatalytic, and photovoltaic devices. *Electrochim. Acta* **128**, 341–348 (2014).
36. Hou, Y., Zhao, Q., Quan, X., Li, X. & Chen, G. Fabrication of Cu₂O/TiO₂ nanotube heterojunction arrays and investigation of its photoelectrochemical behavior. *Appl. Phys. Lett.* **95**, 093108 (2009).
37. Li, Y. S. *et al.* Enhanced photocatalytic activities of TiO₂ nanocomposites doped with water-soluble mercapto-capped CdTe quantum dots. *Appl. Catal. B: Environ* **101**, 118–129 (2010).
38. Wang, Q., Qiao, J., Xu, X. & Gao, S. Controlled synthesis of Cu nanoparticles on TiO₂ nanotube array photoelectrodes and their photoelectrochemical properties. *Mater. Lett.* **131**, 135–137 (2014).
39. Hu, L. H. *et al.* Microstructure design of nanoporous TiO₂ photoelectrodes for dye sensitized solar cell modules. *J. Phys. Chem. B* **111**, 358–362 (2007).
40. Li, G., Dimitrijevic, N. M., Chen, L., Rajh, T. & Gray, K. A. Role of surface/interfacial Cu²⁺ sites in the photocatalytic activity of coupled CuO-TiO₂ nanocomposites. *J. Phys. Chem. C* **112**, 19040–19044 (2008).
41. Luo, J. S. *et al.* TiO₂/(CdS, CdSe, CdSeS) nanorod heterostructures and photoelectrochemical properties. *J. Phys. Chem. C* **116**, 11956–11963 (2012).
42. Sun, Q., Li, Y., Sun, X. M. & Dong, L. F. Improved photoelectrical of single-crystal TiO₂ nanorod arrays by surface sensitization with copper quantum dots. *ACS Sustainable Chem. Eng.* **1**, 798–804 (2013).
43. Tian, H. *et al.* Retarded charge recombination in dye-sensitized nitrogen-doped TiO₂ solar cells. *J. Phys. Chem. C* **114**, 1627–1632 (2010).
44. Cao, J. L. *et al.* Hierarchical meso-macroporous titania-supported CuO nanocatalysts: preparation, characterization and catalytic CO oxidation. *J. Mater. Sci.* **44**, 6717–6726 (2009).
45. Chan, G. H., Zhao, J., Hicks, E. M., Schatz, G. C. & Van Duyne, R. P. Plasmonic properties of copper nanoparticles fabricated by nanosphere lithography. *Nano Lett.* **7**, 1947–1952 (2007).
46. Park, B. K. *et al.* Synthesis and size control of monodisperse copper nanoparticles by polyol method. *J. Colloid Interface Sci.* **311**, 417–424 (2007).
47. Tian, B., Li, C. & Zhang, J. One-step preparation characterization and visible-light photocatalytic activity of Cr-doped TiO₂ with anatase and rutile bicrystalline phases. *Chem. Eng. J.* **191**, 402–409 (2012).
48. Sajjad, A. K. L., Shamaila, S., Tian, B., Chen, F. & Zhang, J. One step activation of WO₃/TiO₂ nanocomposites with enhanced photocatalytic activity. *Appl. Catal. B: Environ* **91**, 397–405 (2009).
49. Hsu, C., Shen, Y., Wei, Z., Liu, D. & Liu, F. Anatase TiO₂ nanobelts with plasmonic Au decoration exhibiting efficient charge separation and enhanced activity. *J. Alloy. Compd.* **613**, 117–121 (2014).
50. Chen, Z., Bercaud, S., Nuckolls, C., Heinz, T. F. & Brus, L. E. Energy transfer from individual semiconductor nanocrystals to graphene. *ACS Nano* **4**, 2964–2968 (2010).
51. Zhang, Y. H., Tang, Z. R., Fu, X. Z. & Xu, Y. J. TiO₂-Graphene nanocomposites for gas-phase photocatalytic degradation of volatile aromatic pollutant: Is TiO₂-graphene truly different from other TiO₂-carbon composite materials? *ACS Nano* **4**, 7303–7314 (2010).
52. Toyoda, T., Hayakawa, T., Abe, K., Shigenari, T. & Shen, Q. Photoacoustic and photoluminescence characterization of highly porous, polycrystalline TiO₂ electrodes made by chemical synthesis. *J. Lumin.* **87**, 1237–1239 (2000).
53. Yu, J., Qi, L. & Jaroniec, M. Hydrogen production by photocatalytic water splitting over Pt/TiO₂ nanosheets with exposed (001) facets. *J. Phys. Chem. C* **114**, 13118–13125 (2010).

54. Yao, H. *et al.* Vertical growth of two-dimensional TiO₂ nanosheets array films and enhanced photoelectrochemical properties sensitized by CdS quantum dots. *Electrochim. Acta* **125**, 258–265 (2014).
55. Zhou, M., Zhou, X. W. D. & Xie, Y. Two-dimensional nanosheets for photoelectrochemical water splitting: Possibilities and opportunities. *Nano Today* **8**, 598–618 (2013).
56. Hodes, G. Comparison of dye- and semiconductor-sensitized porous nanocrystalline liquid junction solar cells. *J. Phys. Chem. C* **112**, 17778–17787 (2008).
57. Yang, L. *et al.* Photoelectrochemical properties of Ag/TiO₂ electrodes constructed using vertically oriented two-dimensional TiO₂ nanosheet array films. *J. Electrochem. Soc.* **163**, H180–H185 (2016).

Acknowledgements

This work was supported by National Natural Science Foundation of China (No. 51472003), State Key Program for Basic Research of China (2013CB632705), the Anhui Provincial Natural Science Foundation (1608085ME95), the Anhui Provincial Natural Science Research Project (KJ2016A524) and the Higher Education Excellent Youth Talents Foundation of Anhui Province (gxyqZD2016328). The authors would like to thank Yonglong Zhuang, Zhongqing Lin, Yun Wu and Chao Cheng of the Experimental Technology Center of Anhui University, for electron microscope test and discussion.

Author Contributions

Jiajia Tao and Zhaoqi Sun wrote the main manuscript text. Miao Zhang prepared Figures 1 and 2. Jianguo Lv prepared Figures 3 and 4. Gang He and Xi Shunjiang prepared Figures 5 and 6. Xiaoshuang Chen prepared Figures 7–9. Yunlang Cheng, Shiwei Shi, Xingzhi Wang, Zhuang Wang, and Zezhou Gong reviewed the manuscript.

Additional Information

Competing Interests: The authors declare that they have no competing interests.

Publisher's note: Springer Nature remains neutral with regard to jurisdictional claims in published maps and institutional affiliations.



Open Access This article is licensed under a Creative Commons Attribution 4.0 International License, which permits use, sharing, adaptation, distribution and reproduction in any medium or format, as long as you give appropriate credit to the original author(s) and the source, provide a link to the Creative Commons license, and indicate if changes were made. The images or other third party material in this article are included in the article's Creative Commons license, unless indicated otherwise in a credit line to the material. If material is not included in the article's Creative Commons license and your intended use is not permitted by statutory regulation or exceeds the permitted use, you will need to obtain permission directly from the copyright holder. To view a copy of this license, visit <http://creativecommons.org/licenses/by/4.0/>.

© The Author(s) 2017